Inorganic Chemistry

Article

pubs.acs.org/IC

Stabilization by Si Substitution of the Pseudobinary Compound $Gd_2(Co_{3-x}Si_x)$ with Magnetocaloric Properties around Room Temperature

Sophie Tencé,*[,†,‡] Rafael Caballero Flores,[†,‡] Johann Chable,[†,‡] Stéphane Gorsse,[†,‡] Bernard Chevalier,[†,‡] and Etienne Gaudin[†,‡]

[†]CNRS, ICMCB, UPR 9048 and [‡]ICMCB, UPR 9048, Université de Bordeaux, F-33600 Pessac, France

Supporting Information

ABSTRACT: We report the discovery of a new solid solution $Gd_2(Co_{3-x}Si_x)$ with $0.29 < x < 0.50$ in the Gd−Co−Si ternary system. Members of this solid solution crystallize with the La_2Ni_3-type structure and correspond to the stabilization of "Gd_2Co_3" through silicon substitution. The structure of the member $Gd_2(Co_{2.53(3)}Si_{0.47})$ was determined by X-ray diffraction on a single crystal. It crystallizes with the space group *Cmce* and cell parameters a = 5.3833(4), b = 9.5535(6), and c = 7.1233(5) Å. Co/Si mixing is observed on two crystallographic positions. All compounds studied in the solid solution present a ferrimagnetic order with a strong composition-dependent Curie temperature T_C with 280 K < T_C < 338 K. The magnetocaloric effect, which amounts to around 1.7 J K^{-1} kg^{-1} for ΔH = 2 T, is interestingly tunable around room temperature over a temperature span of 60 K through only 4−5% of composition change.

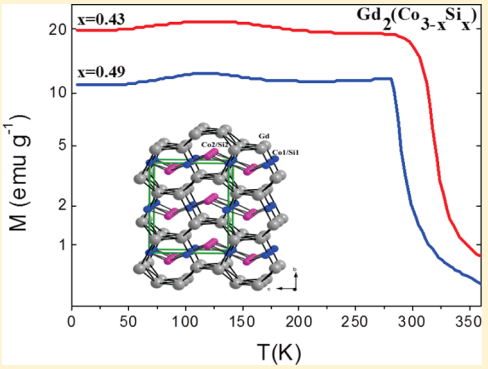

1. INTRODUCTION

The search for new materials for magnetic refrigeration around room temperature is an exciting challenge since the discovery of the large magnetocaloric effect in $Gd_5Ge_2Si_2$.[1] If Mn−Fe−P- and La−Fe−Si-based materials are currently optimized for applications in a near future,[2] investigation of other systems is still relevant. With this in mind, the Gd-rich part of some Gd−M−X (M = d-metal, X = p-metal) ternary systems was studied because of the large magnetic moment of Gd and its isotropic character limiting the magnetic hysteresis. Thus, the system Gd−Co−Si was investigated after the discovery of the new Gd-rich phase $Gd_6Co_{1.67}Si_3$ as secondary phase during the synthesis of a GdCoSi sample.[3] This compound orders ferromagnetically at 294 K and exhibits interesting magnetocaloric properties.[4−6] Thereafter, the Gd_5CoSi_2[7] and $Gd_3Co_{2.48}Si_{1.52}$[8] phases were discovered. Gd_5CoSi_2 adopts the Cr_5B_3-type structure, and $Gd_3Co_{2.48}Si_{1.52}$ adopts the Er_3Ge_4-type structure. They are both characterized by statistical distribution between Co- or Si-atoms on one or two crystallographic sites. No solid solution was observed around the phase Gd_5CoSi_2, which orders ferromagnetically with the Curie temperatures T_C = 168 K. Concerning $Gd_3Co_{2.48}Si_{1.52}$, a phase crystallizing with the same structure and with the composition of $Gd_3Co_{2.2}Si_{1.8}$ was recently reported,[9] suggesting the existence of the solid solution $Gd_3Co_{4-x}Si_x$. However, its homogeneity range has not yet been studied. It should be noticed that although the binary compounds Gd_3Co_4 and Gd_3Si_4 do not exist, the $Gd_3Co_{4-x}Si_x$ phase crystallizes as Gd_3Ge_4[10] with the Er_3Ge_4-type structure. The mix occupancy of silicon and cobalt on some crystallographic positions then allows the stabilization of this structural type. Moreover, it appears that a significant change in the composition between $Gd_3Co_{2.48}Si_{1.52}$ and $Gd_3Co_{2.2}Si_{1.8}$ does not really affect the magnetic properties since they show close ferromagnetic transition temperature with T_C = 180 and 172 K, respectively.

During the study of the phase $Gd_3Co_{2.48}Si_{1.52}$, the new phase $Gd_{40}Co_{51}Si_9$ has been evidenced by electron microprobe analysis.[8] This new phase crystallizes with the La_2Ni_3-type structure. As previously observed with the phase $Gd_2Co_{2.94}Ga_{0.06}$[11] the substitution of a small amount of silicon to cobalt allows stabilizing the pseudo binary phase $Gd_2(Co_{3-x}Si_x)$. The existence of Gd_2Co_3 was never reported, and only a few compounds crystallize with the La_2Ni_3-type structure. One can cite La_2Co_3[12] and Nd_2Co_3.[13] For La_2Co_3, an antiferromagnetic ordering below T_N = 315 K was evidenced by magnetization measurements and confirmed by neutron diffraction on powder. The cobalt atoms on the two crystallographic positions carry a small magnetic moment with a noncollinear magnetic structure.

In this work we show that a solid solution $Gd_2(Co_{3-x}Si_x)$ with $0.29 < x < 0.50$ exists. The study of its magnetic properties reveals a ferrimagnetic ordering for all the samples and a strong dependence of the Curie temperature versus the Si-content. The magnetocaloric properties of the sample, which exhibits a Curie temperature near room temperature, are also determined.

Received: March 10, 2014
Published: June 18, 2014

   dx.doi.org/10.1021/ic500529b | *Inorg. Chem.* 2014, 53, 6728−6736

Table 1. Atomic Positions (x, y, z), Equivalent Displacement Parameters (U_{eq}), and Occupancy (occ) for $Gd_2Co_{2.53(3)}Si_{0.47}$

position	Wyck.	x	y	z	U_{eq} (Å^2)	occ
Gd	8*f*	0	0.33623(2)	0.09712(3)	0.01228(9)	1
Co1[a]	4*a*	0	0	0	0.0123(3)	0.594(10)
Si1[a]	4*a*	0	0	0	0.0123	0.406
Co2[a]	8*e*	1/4	0.08438(6)	1/4	0.0132(2)	0.968(8)
Si2[a]	8*e*	1/4	0.08438	1/4	0.0132	0.032

[a]Atomic coordinates and anisotropic displacement parameters were constrained to be equal.

Table 2. Curie Temperatures (T_C) and Cell Parameters vs Composition (EPMA) for the $Gd_2(Co_{3-x}Si_x)$ Compounds Obtained from a Given Nominal Composition and Annealing Temperature (T_A)

nominal composition	$Gd_{40}Co_{55}Si_5$	$Gd_{40}Co_{51}Si_9$	$Gd_{40}Co_{51}Si_9$	$Gd_{40}Co_{51}Si_9$	$Gd_{40}Co_{45}Si_{15}$	$Gd_{40}Co_{51}Si_9$	$Gd_{40}Co_{51}Si_9$
T_A (K)	1073	773	873	973	1073	1073	1173
composition Gd/Co/Si in atom %	40.4/53.9/5.7	39.7/52.5/7.8	40.0/51.5/8.5	39.8/51.5/8.7	40.5/50.4/9.1	39.9/50.3/9.8	40.5/49.5/10.0
x in $Gd_2Co_{3-x}Si_x$	0.29	0.39	0.43	0.44	0.46	0.49	0.50
T_C (K)	338(2)	327(2)	315(2)	303(2)	288(2)	287(2)	280(2)
a (Å)	5.3623(3)	5.3681(4)	5.3726(4)	5.3748(4)		5.3833(4)	5.3863(4)
b (Å)	9.5711(4)	9.5610(6)	9.5593(6)	9.5558(6)		9.5535(6)	9.5513(6)
c (Å)	7.1312(4)	7.1254(5)	7.1249(5)	7.1245(5)		7.1233(5)	7.1222(5)

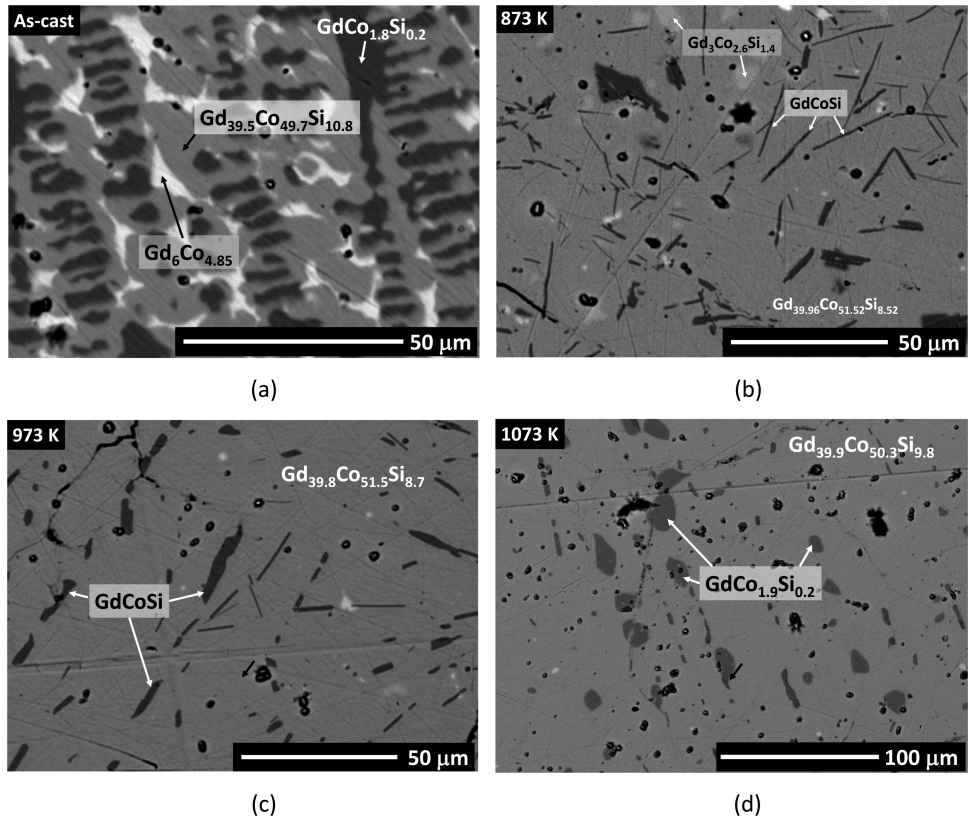

Figure 1. SEM-BSE images of the $Gd_{40}Co_{51}Si_9$ alloy composition in the states (a) as-cast, (b) annealed at 873 K, (c) 973 K, and (d) 1073 K.

2. EXPERIMENTAL DETAILS

Samples with the following nominal compositions $Gd_{40}Co_{51}Si_9$, $Gd_{40}Co_{55}Si_5$, and $Gd_{40}Co_{45}Si_{15}$ were prepared by melting precisely weighted amounts of high purity elements Gd, Co, and Si (99.9%) in an arc melting furnace. Melting was performed three times to ensure a good homogeneity under a purified argon gas atmosphere. The weight losses during the overall melting process were less than 0.3 wt %, and finally the as-cast samples were quenched by switching off the power supply. Then, the as-cast samples were enclosed in evacuated quartz tube and underwent a heat treatment at 1173, 1073, 973, 873 K for one month and at 773 K for seven weeks for $Gd_{40}Co_{51}Si_9$ and five weeks for $Gd_{40}Co_{55}Si_5$ and $Gd_{40}Co_{45}Si_{15}$. No reaction between the sample and the quartz tube was observed.

Both the composition and the homogeneity of the as-cast and annealed samples were checked by microprobe analysis using a Cameca SX-100 instrument. The analysis was performed on the basis of intensity measurements of Gd Lα_1, Co Kα_1, and Si Kα_1 X-ray emission lines, which were compared with those obtained for the equiatomic GdCoSi used as internal reference in the samples (secondary phase).

Routine X-ray powder diffraction was performed with the use of a Philips 1050-diffractometer (Cu Kα radiation) for the characterization of the structural type and for the phase identification of the as-cast and

dx.doi.org/10.1021/ic500529b | Inorg. Chem. 2014, 53, 6728−6736

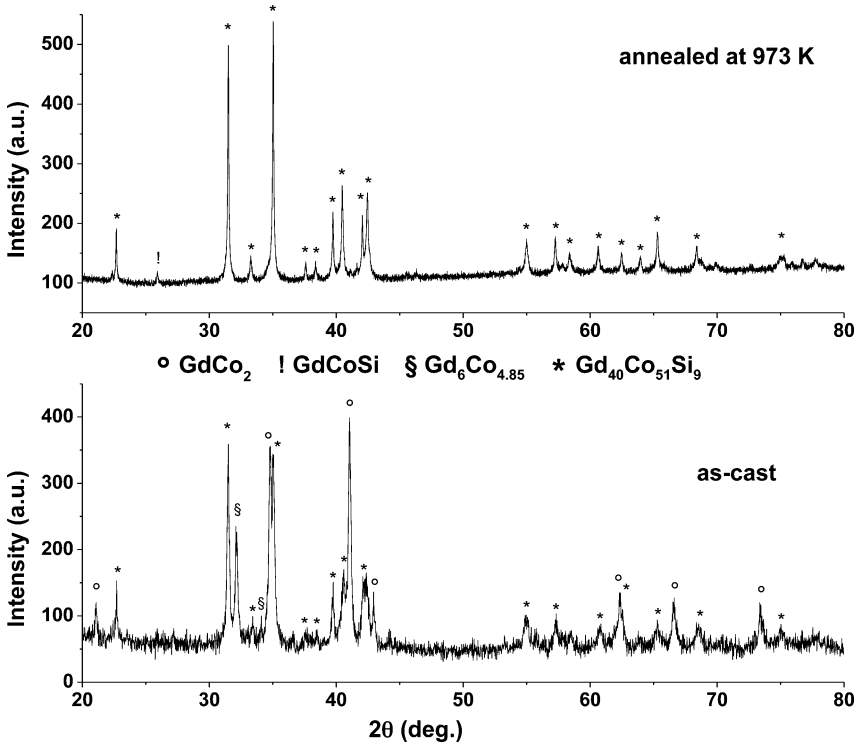

Figure 2. X-ray powder patterns of the "$Gd_{40}Co_{51}Si_9$" sample after melting (as-cast) and after annealing at 973 K leading to $Gd_2(Co_{3-x}Si_x)$ with x = 0.44. The phases are identified by different symbols indicated between both patterns.

annealed samples. X-ray powder data for full pattern matching analysis were collected at room temperature using a PANalytical X'Pert Pro diffractometer working with the Cu Kα_1 radiation (λ = 1.54051 Å) in the range of 12 ≤ 2θ ≤ 130° with a step size of 0.008°. Rietveld refinement was realized by means of the Fullprof program package.[14]

A single crystal was isolated from a crushed block of the sample with nominal composition $Gd_{40}Co_{51}Si_9$ annealed at 1073 K during one month. The refinement of the structure was made from single-crystal X-ray diffraction data collected at room temperature on an Enraf-Nonius Kappa CCD using Mo Kα radiation. A Gaussian-type absorption correction was applied, the shape of the single crystal being determined with the video microscope of the diffractometer. 430 independent reflections were measured up to θ = 35°. All data processing and refinements were performed with the Jana2006 program package.[15] The atomic positions were initially determined using the SUPERFLIP program[16] and the space group *Cmce* (No. 64). A first refinement with only Co atoms on 4*a* and 8*e* positions led to high atomic displacement parameters on 4*a* position. A mixing of Co- and Si-atoms on the two positions confirmed that most of the Si-atoms are located on the 4*a* position (Table 1). As previously observed for $Gd_2Co_{2.94}Ga_{0.06}$, a small amount of Co is substituted on the 8*e* position. Using this disordered model, at the end of the refinement the reliability factors $R[F^2 > 2\sigma(F^2)]$ and $wR(F^2)$ were equal to 0.026/0.052 with goodness of fit S = 1.09 and residual electron density in the range of [−1.19, +1.00 e Å^{-3}]. The chemical composition deduced from this refinement, $Gd_2Co_{2.53(3)}Si_{0.47}$, is very close to the one determined by electron probe microanalysis (EPMA), that is, $Gd_{2.00(2)}Co_{2.52(3)}Si_{0.49(2)}$ (Table 2). Details of data collections, structure refinements, the atomic parameters, and CIF file are listed in Table 1 and Supporting Information.

Magnetization measurements were performed using a superconducting quantum interference device (SQUID) magnetometer (Quantum Design MPMS-XL) in the temperature range of 5−360 K and in fields up to 4.6 T. Susceptibility at high temperature (300−700 K) was measured with an extraction-type magnetometer at 4 T.

Heat capacity was determined with a standard relaxation method with a Quantum Design PPMS device. Sample of approximately 50 mg was glued to the sample holder using Apiezon N-grease. The heat capacity of the sample holder and grease was measured just before the sample was studied.

3. RESULTS AND DISCUSSION

3.1. Microstructural Observation. Figure 1a−d shows the SEM backscattered electron (BSE) images of the alloy $Gd_{40}Co_{51}Si_9$ sample in the (a) as-cast and annealed states at (b) 873 K, (c) 973 K, and (d) 1073 K. In BSE images, the phases of highest mean atomic number (Gd content) appear brightest in the images. Phase identification was made using energy dispersive X-ray (EDX) analysis.

The as-cast sample exhibits a microstructure composed of the $GdCo_{1.8}Si_{0.2}$ (black), $Gd_{39.5(3)}Co_{49.7(6)}Si_{10.8(3)}$ (gray), and $Gd_6Co_{4.85}$ (white) phases. The $GdCo_{1.8}Si_{0.2}$ phase, that is, $Gd(Co_{2-y}Si_y)$ with y = 0.24, being dendritic appears first in the melt during cooling. In addition, it appears that the $Gd_{39.5}Co_{49.7}Si_{10.8}$ phase grows at the expense of the Gd-$(Co_{2-y}Si_y)$ phase. These observations suggest that the formation of this ternary phase involved a peritectic reaction between the liquid and the $Gd(Co_{2-y}Si_y)$ phase.

The results of the microstructure and composition analysis of the samples annealed at 1073, 973, and 873 K evidence in all cases nearly single-phase samples with nevertheless small content of secondary phases, that is, GdCoSi and $Gd_3Co_{2.6}Si_{1.4}$ at 873 K, GdCoSi at 973 K, $Gd(Co_{2-y}Si_y)$ with y = 0.2 at 1073 and 1173 K (not shown). These results suggest that the $Gd_{40}Co_{51}Si_9$ alloy composition is near to the solvus of a one-single solid solution phase field. Interestingly, the composition of the solid solution changes as a function of the annealing temperature, which can be related to the thermal dependence of the solvus.

The microprobe analysis of the as-cast samples of nominal composition $Gd_{40}Co_{55}Si_5$ and $Gd_{40}Co_{45}Si_{15}$ evidence the presence of $Gd_{41.0}Co_{52.3}Si_{6.7}$ in the first one and the absence

dx.doi.org/10.1021/ic500529b | Inorg. Chem. 2014, 53, 6728−6736

of the new phase in the second one suggesting that the composition $Gd_{40}Co_{45}Si_{15}$ cross a different liquid surface. After annealing at 1073 K, the Si-poor and Si-rich alloy compositions lead to a single-phase with composition $Gd_{40.4}Co_{53.9}Si_{5.7}$ and $Gd_{40.5}Co_{50.4}Si_{9.1}$. These compositions are provided in Table 2.

3.2. XRD Analysis. According to X-ray powder diffraction (XRPD) the as-cast $Gd_{40}Co_{51}Si_9$ sample is not single phase: the peaks of the two known phases $GdCo_2$[17] (more exactly $Gd(Co_{2-y}Si_y)$ with $y = 0.2$) and $Gd_6Co_{4.85}$[18] are observed added to extra reflections highlighted with the * symbols in the pattern (Figure 2). This result agrees with the microprobe analysis presented in Figure 1a. The XRPD patterns performed after the different annealings are very similar and also in fair agreement with the microprobe analysis: for example, the diffractogram for the annealed sample $Gd_{40}Co_{51}Si_9$ at 973 K given in Figure 2 contains only reflections marked by * symbols corresponding to the new ternary compound as well as a small amount of the equiatomic GdCoSi whose main peak is around $2\theta = 26°$. The peaks of $GdCo_2$ and $Gd_6Co_{4.85}$ are not distinguishable any more. The reflections of the main phase were indexed with space group *Cmce* and cell parameters $a = 5.3748(4)$, $b = 9.5558(6)$, and $c = 7.1245(5)$ Å (Table 2). These structural data are relatively close to those of La_2Co_3 (space group *Cmce*, $a = 4.886(7)$, $b = 10.34(10)$, and $c = 7.811(5)$ Å)[19] and La_2Ni_3 (space group *Cmce*, $a = 5.113(8)$, $b = 9.731(6)$, and $c = 7.907(5)$ Å)[20] suggesting that the new ternary phase may crystallize with the same type structure and whose formula could be rewritten as $Gd_2(Co_{3-x}Si_x)$ with $x \approx 0.44$ assuming the overall composition of $Gd_{39.8}Co_{51.5}Si_{8.7}$ determined by EPMA (Table 2). Single crystal measurements presented in the next part confirm this assumption with a refined structure yielding the chemical formula of $Gd_{40}Co_{50.6}Si_{9.4}$ or $Gd_2(Co_{3-x}Si_x)$ with $x \approx 0.47$ for an annealing temperature of 1073 K.

Looking more carefully to the micropobe analysis we observe a small deviation of the main-phase composition, that is, the silicon content increases from 5.7 to 10.0 atom %, whereas the cobalt content decreases from 53.9 to 49.5 atom % (see Table 2). To check the assumption of a composition depending significantly on the annealed temperature and nominal composition we carried out a full pattern matching fitting of the X-ray data to determine the unit cell parameters. The evolution of these refined parameters in function of the composition given by the microprobe analysis is plotted in Figure 3 and summarized in Table 2. It appears clearly that the lattice parameters depends on the Si (or Co) content since we observe that a increases (+0.45%) with increasing Si content, whereas b and c decrease (−0.21 and −0.13%, respectively). More generally, if we consider the cell parameters of La_2Co_3, La_2Ni_3 (cf. above), and Nd_2Co_3 ($a = 4.96$, $b = 10.01$, and $c = 7.57$ Å)[13] in respect to those of $Gd_2(Co_{3-x}Si_x)$, it is clear that the rare earth and transition metal strongly influence the lattice parameters of the La_2Ni_3-type compounds.

The cell parameters of $Gd_{40.4}Co_{53.9}Si_{5.7}$ (low Si content) were refined to $a = 5.3623(3)$, $b = 9.5711(4)$, and $c = 7.1312(4)$ Å, in agreement with the tendency of the cell dimension evolution versus Si content (Figure 3). Thus, the limits of the homogeneity range were not precisely established, but our first approach suggests the existence of a solid solution $Gd_2(Co_{3-x}Si_x)$ with approximately $0.29 < x < 0.50$, that is, between 5.7 and 10.0 atom % of silicon. This domain is rather small, but it is sufficient to observe modification of the magnetic properties of the new ternary phase (see below). We can

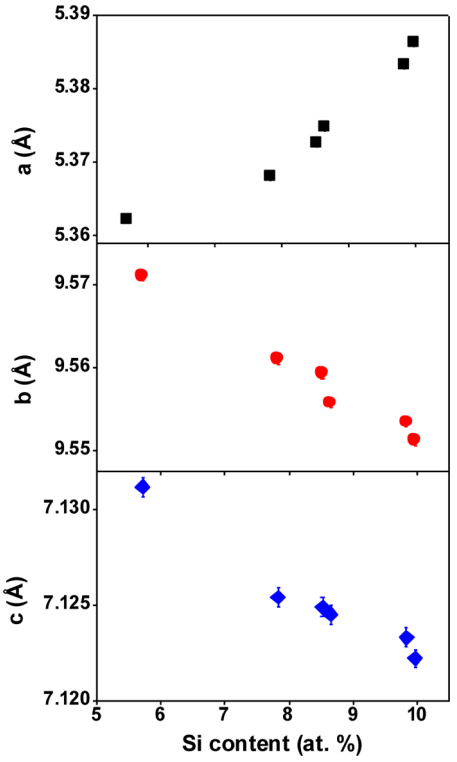

Figure 3. Dependence vs Si content of the unit cell parameters for the $Gd_2(Co_{3-x}Si_x)$ compounds.

conclude that a small amount of silicon allows us to stabilize the pseudobinary $Gd_2(Co_{3-x}Si_x)$.

Figure 4 is a ternary plot summarizing the binary and ternary phases identified in the Gd-rich Co−Si system. In addition to the new phase $Gd_2(Co_{3-x}Si_x)$, which exhibits a homogeneity range and a strong composition-dependent Curie temperature (see below), five ternary compounds were evidenced in the Gd-rich corner. Among them, previous results[8] for the solid solution $Gd_3(Co_{4-x}Si_x)$ suggest a solubility range similar to $Gd_2(Co_{3-x}Si_x)$ but with only a weak dependence on the Curie temperature. In addition to the compounds, the boundary of the projected liquidus surface corresponding to the primary crystallization of $GdCo_2$ was roughly plotted according to the solidification microstructures described in Section 3.1.

3.3. Crystallographic Structure. $Gd_2Co_{2.53(3)}Si_{0.47}$ crystallizes with the La_2Ni_3-type structure.[20] Its crystal structure is made of a three-dimensional framework of Gd atoms and puckered two-dimensional $[Co_{2.53}Si_{0.47}]$ layers aligned along the b axis (Figures 5 and 6). In the Gd framework, channels are running along the a axis and the Gd atoms are located into a square pyramid of Gd (Figure 6). The Gd−Gd distances, which are ranging from 3.421 to 3.463 Å (Table 3), are significantly shorter than the one observed in metallic Gd[21] with $d_{Gd-Gd} = 3.574$ and 3.636 Å but are close to the ones observed in many ternary and binary compounds in the Gd−Co−Si system. For instance, the average Gd−Gd distances in $Gd_6Co_{4.85}$,[18] Gd_5CoSi_2,[22] and $Gd_3Co_{2.48}Si_{1.52}$[8] are equal to 3.382, 3.424, and 3.526 Å, respectively, and are ranging from 3.324 to 3.909 Å in $Gd_{12}Co_7$.[23] In the $[Co_{2.53}Si_{0.47}]$ layers, the Co and Si atoms form a kagome-like lattice (Figure 6). The distance between two consecutive layers is equal to $b/2 = 4.777$ Å. In the hexagonal rings the Co1/Si1−Co2/Si2 and Co2/Si2−Co2/Si2 distances are equal to 2.373 and 2.692 Å, respectively. The

dx.doi.org/10.1021/ic500529b | Inorg. Chem. 2014, 53, 6728−6736

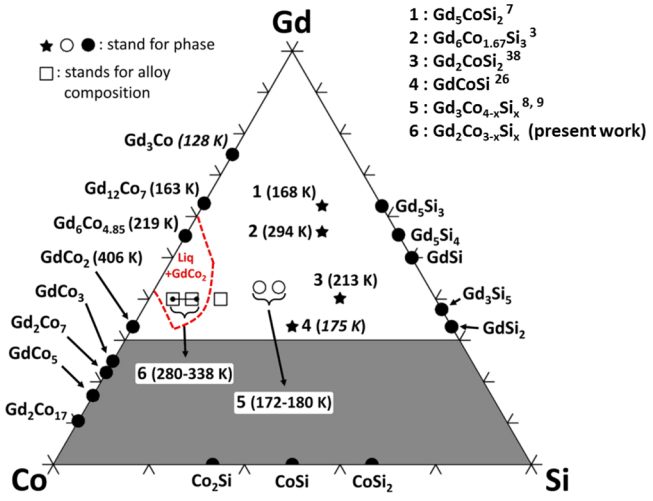

Figure 4. Ternary diagram showing the composition of the binary and Gd-rich ternary phases in the Gd−Co−Si system. Curie and Néel temperatures of the phases are indicated in brackets in roman and italic, respectively. Square symbols stand for the experimental alloy compositions prepared in the present study, whereas the line delimited by the brace shows the homogeneity range of the $Gd_2Co_{3-x}Si_x$ compound determined at 773−1173 K. The red dashed line represents the probable locus of the univariant transformation delimitating the liquidus surface Liq + $GdCo_2$. This univariant line is drawn by extrapolation of the invariant peritectic reactions Liq + $GdCo_3$ ⇔ $GdCo_2$ and Liq + $GdCo_2$ ⇔ $Gd_6Co_{4.85}$ and passing between our two experimental alloy composition as discussed in Section 3.1.

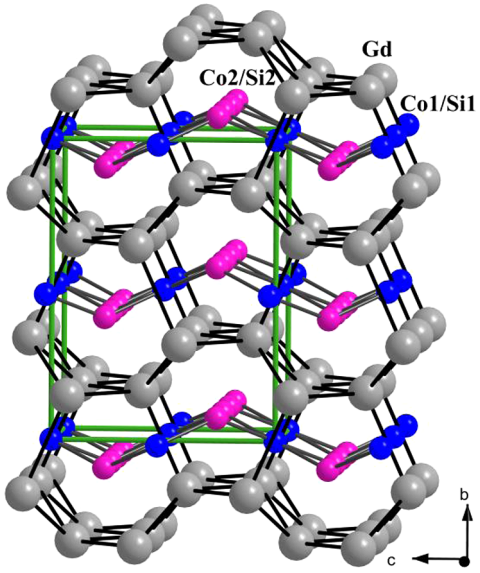

Figure 5. View of the crystal structure of $Gd_2Co_{2.53(2)}Si_{0.47}$. The Gd−Gd and Co/Si−Co/Si bonds are drawn.

shortest distance is equal to the sum of the covalent radii (r_{Si} + r_{Co} = 1.11 + 1.26 = 2.37 Å).[24] The second distance is rather long compared to the sum of the covalent or metallic radii. This difference in between the two distances was previously observed in the homologous compound $Gd_2Co_{2.94}Ga_{0.06}$[11] with the values of 2.348 and 2.658 Å. In the case of the binary compound La_2Co_3,[12] the similar Co−Co distances are equal to 2.427 and 2.471 Å. In these latter cases the kagome-like Co layers are made of almost regular hexagonal rings. The Co−Co−Co angles are equal to 119.4 or 121.2° in La_2Co_3 and to 110.9 and 124.5° for the Co2−Co1−Co2 and Co1−Co2−Co2 angles in $Gd_2Co_{2.53(3)}Si_{0.47}$. The strong distortion of the hexagonal rings can be attributed to the nature of the rare-earth metal since a strong distortion is also observed for $Gd_2Co_{2.94}Ga_{0.06}$, which contains only a small amount of Ga. This distortion is correlated to the significant changes in cell parameters when going from La_2Co_3 to $Gd_2Co_{3-x}Si_x$. The coexistence of a three-dimensional framework of Gd atoms and two-dimensional covalent layers made of Co and Si atoms was previously observed in $Gd_3Co_{2.48}Si_{1.52}$.[8] For this latter compound the Co−Co/Si distances equal to 2.418 and 2.469 Å and Co−Co distances to 2.531 Å are close to the ones observed in $Gd_2Co_{2.53(3)}Si_{0.47}$.

3.3. Magnetic and Magnetocaloric Properties.

3.3.1. Magnetization Measurements. Figure 7 presents the temperature dependence of the specific magnetization $M(T)$ at low field ($\mu_0 H$ = 0.05 T) of the annealed samples $Gd_2(Co_{3-x}Si_x)$ obtained from the $Gd_{40}Co_{51}Si_9$ nominal composition. The multiphase character of the as-cast sample (not shown) is evidenced by the existence of three different drops in the M versus T curve associated with the presence of the binary compound $Gd_6Co_{4.85}$ (T_C = 219 K),[18] $Gd(Co_{2-y}Si_y)$ (y = 0.2) (T_C around 350−400 K according to y value),[25] and the main phase $Gd_{1.98}Co_{2.49}Si_{0.54}$. The magnetization curves of the annealed samples indicate the disappearance of the multiphase character with well-defined drops in the M versus T curves at the Curie temperature T_C of the main phases. The different T_C values are related to the slight change in the chemical composition achieved by different heat treatments, as mentioned in the previous section. The origin of the weak bump in the magnetization curves observed for the annealed samples around 150 K cannot be attributed to the minority phase GdCoSi since its Néel temperature T_N = 175 K is too far from the anomaly.[26] This could be from intrinsic origin to the new $Gd_2(Co_{3-x}Si_x)$ phase, possibly due to a spin reorientation. The values of T_C have been obtained from the inflection point of the experimental magnetization data at low field (see Figure 7) and are gathered in Table 2. As it is presented, a change in the annealing temperature can be used to tune T_C in the vicinity of room temperature via the modification of the ratio Co/Si content.

The compositional evolution of the experimental T_C of the different $Gd_2(Co_{3-x}Si_x)$ samples has been precisely studied as a function of the Co (Figure 8, upper) and Si (Figure 8, lower) contents. The composition of the annealed samples was analyzed by EPMA in several regions of the sample showing good homogeneity. As can be seen in both panels of Figure 8, the initial composition of the $Gd_{1.98}Co_{2.49}Si_{0.54}$ as-cast sample is recovered as the annealing temperature T_A increases: a nearly linear behavior is observed in the Co (Si) content that decreases (increases) with increasing T_A. It is worth mentioning that the Gd content is almost constant (∼40 atom %, the nominal value) both in the main phases of the as-cast as well as the annealing samples (not shown in Figure 8). The Curie temperature decreases when cobalt is replaced by silicon as observed for $Gd(Co_{2-y}Si_y)$.[25] It is clear that the variation of T_C cannot be ascribed to a structural effect since the interatomic distances barely change with the composition (see previous section). It arises more likely from the electronic effect since the p(Si)−d(Co) hybridization increases when Co is doped by Si, which modifies the Co magnetic moment. According to density functional theory calculation performed on Gd-$(Co_{2-y}Si_y)$ by Burzo et al.,[25] the peaks of Co(d) density of

dx.doi.org/10.1021/ic500529b | Inorg. Chem. 2014, 53, 6728−6736

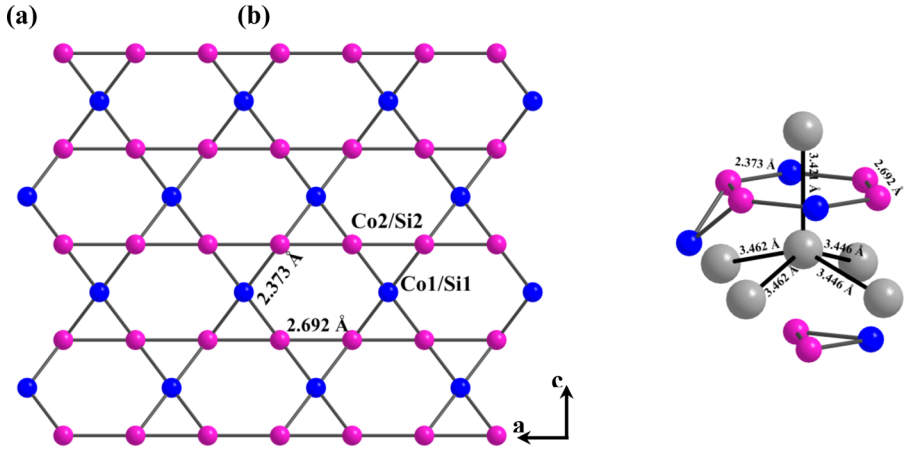

Figure 6. (a) View of the kagome-like Co/Si two-dimensional layer along the *b* axis. (b) Local environment of Gd atoms. The atoms in the Gd, Co1/Si1, and Co2/Si2 positions are drawn in gray, blue, and pink, respectively.

Table 3. Interatomic Distances in Å for $Gd_2Co_{2.53(3)}Si_{0.47}$

Gd	Co2/Si2 × 2	2.9156(4)	Co1/Si1	Co2/Si2 × 4	2.3733(3)
	Co2/Si2 × 2	2.9355(6)		Gd × 4	3.1893(4)
	Co2/Si2 × 2	2.9642(6)		Gd × 2	3.2686(4)
	Co1/Si1 × 2	3.1893(4)		Gd × 2	3.2858(4)
	Co1/Si1 × 1	3.2686(4)			
	Co1/Si1 × 1	3.2858(4)	Co2/Si2	Co1/Si1 × 2	2.3733(3)
	Gd × 1	3.4214(5)		Co2/Si2 × 2	2.6916(4)
	Gd × 2	3.4459(4)		Gd × 2	2.9156(4)
	Gd × 2	3.4625(4)		Gd × 2	2.9355(6)
				Gd × 2	2.9642(6)

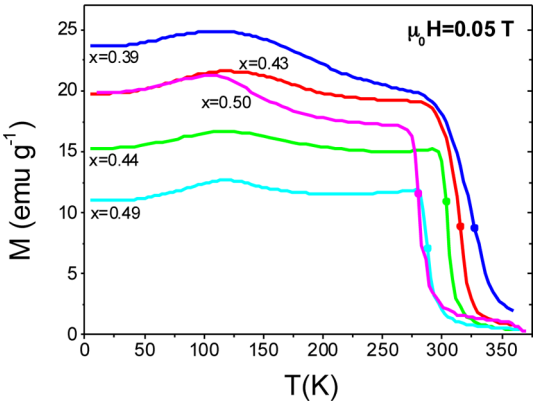

Figure 7. Temperature dependence of the magnetization of the $Gd_2(Co_{3-x}Si_x)$ samples obtained from the preparation with the nominal composition $Gd_{40}Co_{51}Si_9$ (see text for the corresponding temperatures of annealing). Filled circles (●) mark the Curie temperature T_C of the samples, i.e., 327(2), 315(2), 303(2), 287(2), and 290(2) for x = 0.39, 0.43, 0.44, 0.49, and 0.50, respectively.

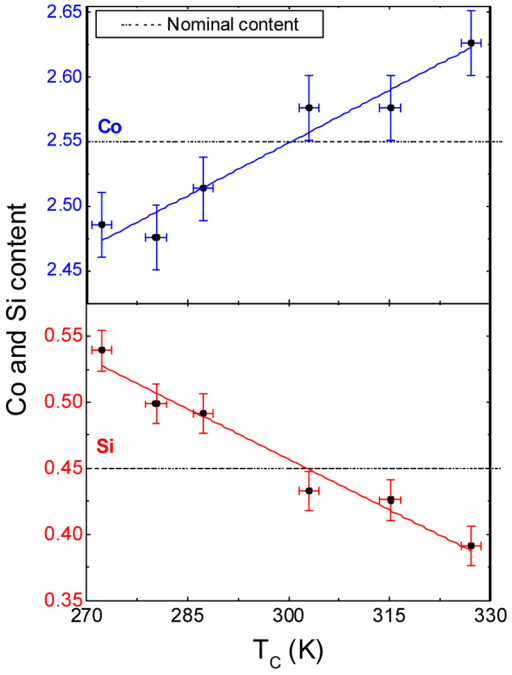

Figure 8. Co (upper) and Si (lower) content dependences of the Curie temperature T_C of the $Gd_2(Co_{3-x}Si_x)$ samples obtained from the preparation with the nominal composition $Gd_{40}Co_{51}Si_9$. Dash-dotted lines indicate the nominal concentrations of Co and Si (51 and 9 atom %, respectively).

states near the Fermi level decrease in intensity and are broadened by p(Si)−d(Co) hybridization, and in addition the Co 3d band is shifted to lower energy. This leads to a diminution of the Co moment as well as the exchange interactions resulting in a decrease of the Curie temperatures.

The study of the magnetic behavior in terms of the magnetic moments of Gd and Co species of the studied $Gd_2(Co_{3-x}Si_x)$ samples was carried out by means of the saturation of $M(H)$ at low temperature and $M(T)$ measurements in the paramagnetic state.

Figure 9 shows in its main panel the field dependence of the magnetization at low temperature (T = 5 K) of the

dx.doi.org/10.1021/ic500529b | Inorg. Chem. 2014, 53, 6728−6736

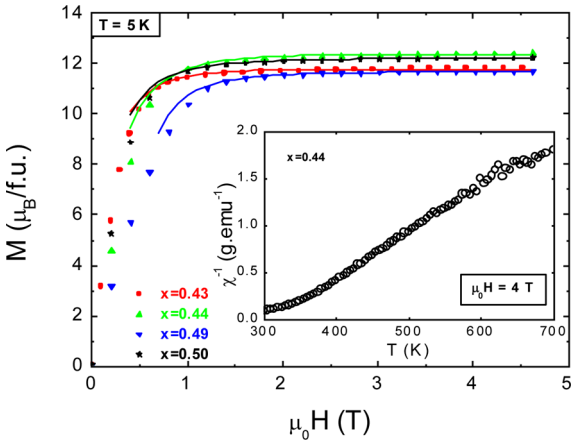

Figure 9. Field dependence, at T = 5 K, of the magnetization of the $Gd_2(Co_{3-x}Si_x)$ samples (symbols + dot lines). Solid lines are the fit of the data using the law of approach to ferromagnetic saturation (see text). (inset) Temperature dependence of the reciprocal susceptibility of the sample $Gd_{1.99}Co_{2.58}Si_{0.44}$.

$Gd_2(Co_{3-x}Si_x)$ samples and indicates similar process to get the saturation values in the whole set of annealed samples except for x = 0.49. For the analysis of the field dependence of the magnetization of the studied $Gd_2(Co_{3-x}Si_x)$ samples, the empirical law of the approach to ferromagnetic saturation M_S can be used.[27,28] This law is valid for fields high enough, when the wall motion is complete and when only magnetization rotation is occurring. The fits of the experimental data $M(H)$ (as can been seen in Figure 9 with solid lines) provide the following M_S fitted values: M_s = 11.92 μ_B (x = 0.43), M_s = 12.66 μ_B (x = 0.44), M_s = 11.66 μ_B (x = 0.49), and M_s = 12.36 μ_B (x = 0.50). The Gd magnetic moment being equal to 7 μ_B or slightly more, at least we would expect a magnetization of 14 μ_B/formula unit (f.u.) if only Gd atoms carry a magnetic moment. Thus, we can conclude that in all samples the Co bears a magnetic moment that is oriented antiparallel to the Gd one, providing in ferrimagnetic ordered compounds. This is usually observed for compounds with cobalt and heavy rare-earth elements. Assuming a magnetic moment of free Gd-atoms $\mu(Gd^{3+})$ = 7 μ_B, the estimation of the minimum contribution per Co atom (average of the two Wyckoff sites moments) to the ferrimagnetic ordered state can be obtained, that is, μ(Co) = 0.81 μ_B (x = 0.43), μ(Co) = 0.52 μ_B (x = 0.44), μ(Co) = 0.93 μ_B (x = 0.49), and μ(Co) = 0.66 μ_B (x = 0.50). The lack of correlation between the chemical composition and the Co moment values is ascribed to the difference of sample purity, which is more significant than the composition variation between samples (around 1−2 atom % only). The average value of the cobalt moment for the four samples is μ(Co) = 0.73 μ_B, keeping in mind that this value could be higher in case of a possible additional contribution of the 5d(Gd) electrons to the total Gd magnetic moment. This value has been compared to the Co magnetic moment in the Gd−Co binary compounds where an increase of the Gd content results in the decrease of the Co magnetic moment:[29] μ(Co) = 1.02 μ_B in $GdCo_2$ (the preceding binary compound with lower Gd content) and μ(Co) = 0.66 μ_B in Gd_4Co_3 (the following one with higher Gd content). Although the binary compound Gd_2Co_3 does not exist, the Co magnetic moment in $Gd_2(Co_{3-x}Si_x)$ is coherent with its intermediate Gd/Co content ratio compared to those of $GdCo_2$ and Gd_4Co_3. Also, it is interesting to note that the cobalt mean magnetic moment value in La_2Co_3 isotype compound (T_N = 315 K) amounts to 0.73 μ_B.[12] The noncollinear magnetic structure of La_2Co_3 consists in canted ferromagnetic puckered layers of Co atoms antiferromagnetically coupled along the b axis.

The inset of Figure 9 shows the experimental values of the reciprocal magnetic susceptibility of the $Gd_{1.99}Co_{2.58}Si_{0.44}$ sample. There is no clear linear behavior of the $\chi^{-1}(T)$ curve above the Curie temperature, and thus the use of the Curie−Weiss law was not considered. Likewise, the fit of $\chi^{-1}(T)$ with the Néel law[30] to take into account the downward curvature of the data was not conclusive. Further susceptibility measurements at higher temperatures will be necessary to reach the linear regime of $\chi^{-1}(T)$ and extract the correct Curie constant as well as the cobalt effective moment.

3.3.2. Specific Heat of $Gd_{1.99}Co_{2.58}Si_{0.44}$ and $Gd_{2.00}Co_{2.52}Si_{0.49}$. To confirm the magnetization data and to calculate the adiabatic temperature change induced by the magnetocaloric effect, we performed specific heat measurement for two selected compositions corresponding to x = 0.44 and 0.49. Figure 10 shows the reduced molar heat capacity at zero

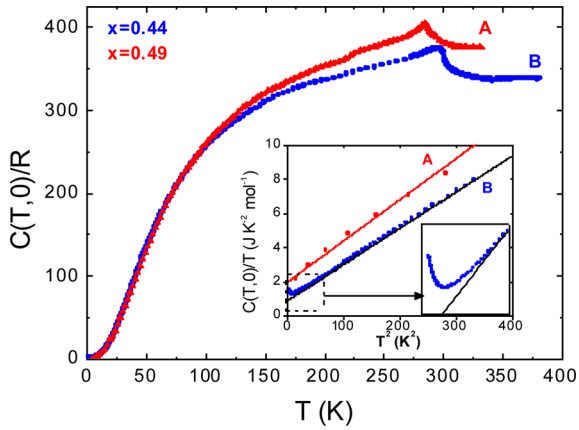

Figure 10. Temperature dependence of the reduced molar heat capacity $C(T, 0)/R$ of $Gd_{2.00}Co_{2.52}Si_{0.49}$ (solid red symbols ▲, denoted as sample A) and $Gd_{1.99}Co_{2.58}Si_{0.44}$ (solid blue symbols ●, denoted as sample B). (inset) Plot of $C(T, 0)/T$ versus T^2. Lines are the low-temperature linear fits (from $C/T = \gamma + \beta T^2$, with γ_A = 20(4) mJ K^{-2} mol(at)$^{-1}$ and γ_B = 9.1(2) mJ K^{-2} mol(at)$^{-1}$).

field $C(T, 0)/R$ of $Gd_{2.00}Co_{2.52}Si_{0.49}$ (solid red symbols ▲, denoted as sample A) and $Gd_{1.99}Co_{2.58}Si_{0.44}$ (solid blue symbols ●, denoted as sample B), with R = 8.31 J K^{-1} mol^{-1} the gas constant. As can be seen, the experimental heat capacity curves of both annealed samples exhibit a clear λ-type peak at T^{λ}_{pkA} = 285(1) K and T^{λ}_{pkB} = 297(1) K for the samples A and B, respectively. This anomaly is associated with a second-order phase transition from paramagnetic (PM) to ferrimagnetic (FM) state at temperatures corresponding to those determined by magnetization measurements, that is, T_{CA} = 287(2) K and T_{CB} = 303(2) K. Considering the conduction electrons and phonons contributions to the heat capacity, the Sommerfeld coefficient γ and the Debye temperature θ_D were determined through the C/T versus T^2 representation derived from the T^3 Debye law at low temperatures.[31] The inset of Figure 10 presents the low-temperature ($T \ll \theta_D$) linear fits of $C/T(T^2)$, which correspond to the fitting parameters γ_A = 20(4) mJ K^{-2} mol(at)$^{-1}$, γ_B = 9.1(2) mJ K^{-2} mol(at)$^{-1}$, θ_{DA} = 239(4) K, and θ_{DB} = 228(4) K. As can be seen in the expanded view shown in the inset of Figure 10, the C/T versus T^2 representation for the

dx.doi.org/10.1021/ic500529b | Inorg. Chem. 2014, 53, 6728−6736

sample $Gd_{1.99}Co_{2.58}Si_{0.44}$ presents an upward deviation below 4 K that has not been considered in the fitting procedure. This deviation of the low-temperature linear behavior has been also found in the literature in Gd-based intermetallic compounds[32] and needs further study. The specific heat for $Gd_{2.00}Co_{2.52}Si_{0.49}$ (sample A) was not measured to such a low temperature, and hence this upward deviation was not observed.

3.3.3. Magnetocaloric Effect of $Gd_{1.99}Co_{2.58}Si_{0.44}$ and $Gd_{2.00}Co_{2.52}Si_{0.49}$. Since these two samples present second-order phase transitions, to evaluate the the magnetocaloric effect (MCE) we calculated the $\Delta S_M(T, H)$ from a family of magnetization isotherms $M(H)$ curves using the numerical resolution of the Maxwell relation. The temperature dependence of ΔS_M obtained for a magnetic field variation between 0 and 2 T is plotted in Figure 11 for $Gd_{1.99}Co_{2.58}Si_{0.44}$ (top) and $Gd_{2.00}Co_{2.52}Si_{0.49}$ (bottom). Both curves have a caretlike shape, characteristic of a second-order phase transition. $-\Delta S_M$ reaches the value of around 1.7 J K^{-1} kg^{-1} for ΔH = 2 T for both samples, but the maximum is observed around 301 K for sample A and 282 K for sample B, that is, close to their respective Curie temperatures. The maximum of MCE, which corresponds to 2.6 J K^{-1} kg$(Gd)^{-1}$ for ΔH = 2 T, is slightly smaller than those of other Gd−Co compounds as $Gd_6Co_{4.85}$ (3.1 J K^{-1} kg$(Gd)^{-1}$),[18] $Gd_{12}Co_7$ (5.6 J K^{-1} kg$(Gd)^{-1}$),[33] or $GdCo_2$ (4.8 J K^{-1} kg$(Gd)^{-1}$).[34]

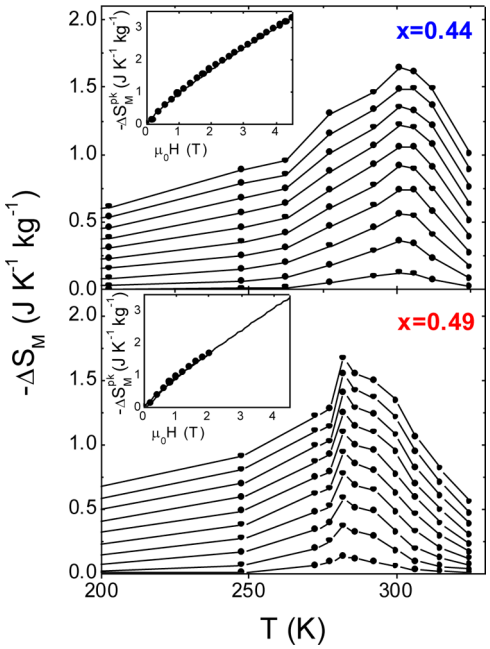

Figure 11. Temperature dependence of the isothermal magnetic entropy change ΔS_M of the samples $Gd_{1.99}Co_{2.58}Si_{0.44}$ (upper) and $Gd_{2.00}Co_{2.52}Si_{0.49}$ (lower) for different values of the magnetic field from 0.2 to 2 T (ΔH = 0.2 T). Lines are guides for the eyes. (insets) Field dependence of the maximum of the magnetic entropy change values ΔS_M^{pk}. Solid lines are the fits as a power law of the experimental data.

The field dependence of the maximum of the magnetic entropy change ΔS_M^{pk} is also shown in inset of Figure 11. It has been shown theoretically and experimentally[35−37] that ΔS_M^{pk} can be expressed as $-\Delta S_M^{pk}(H) = cH^n$, with n field independent at $T = T_C$. The fit of the experimental data with the power law gives the fitting parameters c_A = 0.92(2), n_A = 0.88(2), c_B = 0.95(2), and n_B = 0.83(2) for samples A and B, respectively. The values of ΔS_M^{pk} for the sample B, fitted from 0 to 2 T according to the mentioned power law, were extrapolated until the same maximum experimental field value 4.5 T applied to the sample A, for comparison. As expected, both samples present similar critical exponent n, but different from the 2/3 value predicted by the mean field theory for materials that undergo second-order transition.

Finally, to fully characterize the MCE in the studied samples A and B, we calculated the adiabatic temperature change $\Delta T_{ad} = [T(S, H) - T(S, 0)]_S$ from $\Delta S_M(T, H)$ and the specific heat measurement at zero field. The temperature dependence of ΔT_{ad} is shown in Figure 12 for the sample B (solid symbols in Figure 12, upper panel) and the sample A (solid symbols in Figure 12, lower panel). Both curves present the characteristic shape that corresponds to a second-order phase transition. Alternatively, the adiabatic temperature change ΔT_{ad} was directly calculated from the expression $\Delta T_{ad}(T, H) \approx -(T/C(T, 0))\Delta S_m(T, H)$, considering $C(T, H) \approx C(T, 0)$. As can be seen in Figure 12 by solid lines, this approximation gives values of ΔT_{ad} in a good agreement with those obtained from the above-mentioned calculation. Likewise, the field dependence of the maximum of the adiabatic temperature change ΔT_{ad}^{pk} was deduced (insets of Figure 12) and fitted with a power law as for ΔS_M^{pk}. The values of the fit were found to be equal to c_A = 0.73(2), n_A = 0.85(2), c_B = 0.93(2), and n_B = 0.82(2). The values of ΔT_{ad}^{pk} for the sample B, fitted from 0 to 2 T according to the mentioned power law, were extrapolated until the same maximum experimental field value 4.5 T applied to the sample A, for comparison.

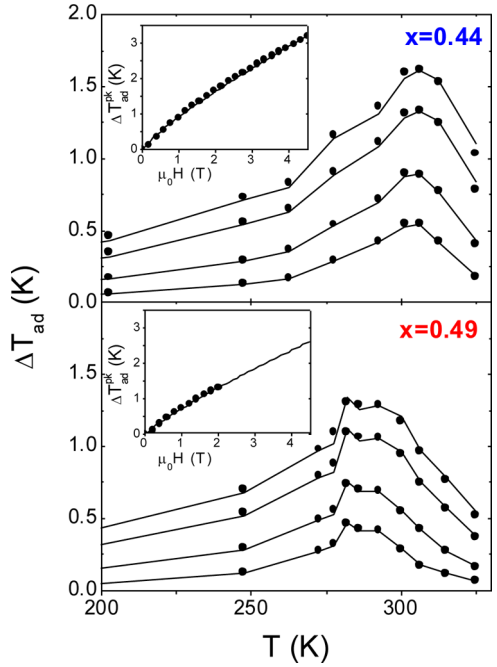

Figure 12. Temperature dependence of the adiabatic temperature change ΔT_{ad} of the samples $Gd_{1.99}Co_{2.58}Si_{0.44}$ (top) and $Gd_{2.00}Co_{2.52}Si_{0.49}$ (bottom) for different values of the magnetic field (0.5, 1, 1.5, and 2 T). The meaning of the solid lines is discussed in the text. (insets) Field dependence of the maximum of the adiabatic temperature change values ΔT_{ad}^{pk}. Solid lines are the fits as a power law of the experimental data.

dx.doi.org/10.1021/ic500529b | Inorg. Chem. 2014, 53, 6728−6736

4. CONCLUSION

This study shows that, although Gd_2Co_3 does not exist, the solid solution $Gd_2(Co_{3-x}Si_x)$ can be stabilized by substituting a small amount of cobalt by silicon. The existence of the solid solution was evidenced by EPMA and XRD measurements, and the homogeneity range is roughly evaluated for x values between 0.29 and 0.50.

The $Gd_2(Co_{3-x}Si_x)$ pseudobinaries undergo a ferrimagnetic transition around room temperature with a Curie temperature that gradually grows from 280 to 338 K with increasing cobalt content. It is noteworthy that only 4−5% of composition change induces a T_C variation over a temperature range of 60 K. This evolution of T_C is ascribed to the electronic effect since the Co moment value is modified via p(Si)−d(Co) hybridization effect and hence the exchange interactions as well.

The magnetocaloric effect amounts to around 1.7 J K^{-1} kg^{-1} for ΔH = 2 T, and the Curie temperature is situated around room temperature as expected for cooling applications. Besides, we found an interesting way to tune the T_C by changing the temperature of the heat treatment inducing a slight change of composition.

■ ASSOCIATED CONTENT

Ⓢ Supporting Information

Two tables giving the details on the structural refinement and the atomic displacement parameters of $Gd_2Co_{2.53(3)}Si_{0.47}$. This material is available free of charge via the Internet at http://pubs.acs.org. The crystallographic information file (CIF) regarding $Gd_2Co_{2.53(3)}Si_{0.47}$ was deposited in the Fachinformationszentrum Karlsruhe (FIZ, 76344 Eggenstein-Leopoldshafen (Germany) with reference CSD-427355.

■ AUTHOR INFORMATION

Corresponding Author

*E-mail: tence@icmcb-bordeaux.cnrs.fr.

Notes

The authors declare no competing financial interest.

■ ACKNOWLEDGMENTS

This work was supported by the ANR (Agence Nationale pour la Recherche) through the research project "MAGCOOL" (ANR-2010-STKE-008).

■ REFERENCES

(1) Pecharsky, V. K.; Gschneidner, K. A. *Phys. Rev. Lett.* **1997**, *78*, 4494−4497.
(2) Sandeman, K. G. *Scr. Mater.* **2012**, *67*, 566−571.
(3) Gaudin, E.; Weill, F.; Chevalier, B. *Z. Naturforsch.* **2006**, *61b*, 825−832.
(4) Gaudin, E.; Tencé, S.; Weill, F.; Rodriguez-Fernandez, J.; Chevalier, B. *Chem. Mater.* **2008**, *20*, 2972−2979.
(5) Shen, J.; Li, Y. X.; Dong, Q. Y.; Wang, F.; Sun, J. R. *Chin. Phys. B* **2008**, *17*, 2268−2271.
(6) Jammalamadaka, S. N.; Mohapatra, N.; Das, S. D.; Iyer, K. K.; Sampathkumaran, E. V. *J. Phys.: Condens. Matter.* **2008**, *20*, 425204(1−6).
(7) Mayer, C.; Gaudin, E.; Gorsse, S.; Chevalier, B. *J. Solid State Chem.* **2011**, *184*, 325−330.
(8) Gaudin, E.; Mayer, C.; Weill, F.; Chevalier, B. *J. Alloys Compd.* **2012**, *545*, 148−152.
(9) Yao, J.; Morozkin, A. V.; Mozharivkyj, Y. *J. Alloys Compd.* **2013**, *550*, 331−334.
(10) Tobash, P. H.; DiFilippo, G.; Bobev, S.; Hur, N.; Thompson, J. D.; Sarrao, J. L. *Inorg. Chem.* **2007**, *46*, 8690−8697.
(11) Sichevich, O. M. *Dopov. Akad. Nauk. Ukr. RSR, Ser. B* **1984**, *12*, 47−49.
(12) Gignoux, D.; Lemaire, R.; Mendia-Monteroso, R.; Moreau, J. M.; Schweizer, J. *Phys. B* **1985**, *130*, 376−378.
(13) Ray, A. E.; Biermann, A. T.; Harmer, R. S.; Davison, J. E. *Cobalt* **1973**, *4*, 103−106.
(14) Rodriguez-Carvajal, J. *Satellite Meeting, 15th IUCr Congress on Powder Diffaction (Toulouse);* IUCR: Chester, England, 1990, 127−128.
(15) Petricek, V.; Dusek, M.; Palatinus, L. *Jana2006, The Crystallographic Computing System;* Institute of Physics: Praha, Czech Republic, 2006.
(16) Palatinus, L.; Chapuis, G. *J. Appl. Crystallogr.* **2007**, *40*, 786−790.
(17) Baenziger, N. C.; Moriarty, J. L., jr. *Acta Crystallogr.* **1961**, *14*, 948−950.
(18) Tencé, S.; Gaudin, E.; Chevalier, B. *Intermetallics* **2010**, *18*, 1216−1221.
(19) Buschow, K. H. J.; Velge, W. A. J. J. *J. Less-Common Met.* **1967**, *13*, 11−17.
(20) Van Vucht, J. H. N.; Buschow, K. H. J. *J. Less-Common Met.* **1976**, *46*, 133−138.
(21) Spedding, F. H.; Daane, A. H.; Herrmann, K. W. *Acta Crystallogr.* **1956**, *9*, 559−563.
(22) Mayer, C.; Gaudin, E.; Gorsse, S.; Chevalier, B. *J. Solid State Chem.* **2011**, *184*, 325−330.
(23) Adams, W.; Moreau, J.-M.; Parthé, E.; Schweitzer, J. *Acta Crystallogr., Sect. B* **1976**, *32*, 2697−2699.
(24) Cordero, B.; Gomez, V.; Platero-Prats, A. E.; Reves, M.; Echeverria, J.; Cremades, E.; Barragan, F.; Alvarez, S. *Dalton Trans.* **2008**, *21*, 2832−2838.
(25) Burzo, E.; Tetean, R.; Sarkozi, Zs.; Chioncel, L.; Neumann, M. *J. Alloys Compd.* **2001**, *323*, 490−493.
(26) Welter, R.; Venturini, G.; Ressouche, E.; Malaman, B. *J. Alloys Compd.* **1994**, *210*, 279−286.
(27) Cullity, B. D.; and Graham, C. D. *Introduction to Magnetic Materials,* 2nd ed.; John Wiley & Sons: New York, 2009; p 325.
(28) Holstein, T.; Primakoff, H. *Phys. Rev.* **1940**, *58*, 1098−1113.
(29) Burzo, E. *Phys. Rev. B* **1972**, *6*, 2882−2887.
(30) Néel, L. *Ann. Phys. (Paris, Fr.)* **1948**, *3*, 137−198.
(31) Kittel, C. *Introduction to Solid State Physics,* 6th ed; Wiley: New York, 1986; pp 106−8, 139.
(32) Seixas, T. M.; Salgueiro da Silva, M. A.; de Lima, O. F.; Lopez, J.; Braun, H. F.; Eska, G. *J. Phys.: Condens. Matter* **2010**, *22*, 136002(1−6).
(33) Chen, X.; Zhuang, Y. H. *Solid State Commun.* **2008**, *148*, 322−325.
(34) Gu, Z.; Zhou, B.; Li, J.; Ao, W.; Cheng, G.; Zhao, J. *Solid State Commun.* **2007**, *141*, 548−550.
(35) Shen, T. D.; Schwarz, R. B.; Coulter, J. Y.; Thompson, J. D. *J. Appl. Phys.* **2002**, *91*, 5240−5245.
(36) Franco, V.; Blázquez, J. S.; Conde, A. *Appl. Phys. Lett.* **2006**, *89*, 222512(1−3).
(37) Franco, V.; Conde, A.; Kuz'min, M. D.; Romero-Enrique, J. M. *J. Appl. Phys.* **2009**, *105*, 07A917(1−3).
(38) Morozkin, A. V.; Yao, J.; Mozharivskyj, Y. *Intermetallics* **2012**, *21*, 115−120.